#### **PAPER**

## Hybrid silicon honeycomb/organic solar cells with enhanced efficiency using surface etching

To cite this article: Ruiyuan Liu et al 2016 Nanotechnology 27 254006

View the article online for updates and enhancements.

#### You may also like

 Mathematical Modeling of the Gas-Phase Chemistry in the Decomposition of Chlorosilanes in Mixtures of Carbon Dioxide and Hydrogen at High Temperatures

Stephanos F. Nitodas and Stratis V. Sotirchos

- Finding the Optimum Chloride-Based Chemistry for Chemical Vapor Deposition of SiC

Milan Yazdanfar, Örjan Danielsson, Olle Kordina et al.

 Deposition-Free Process on Reactor Sidewalls during Si Deposition in Vertical Rotating Disk Reactors
 Soichiro Makino, Kenji Nakashima and Masahide Inagaki



### IOP ebooks™

Bringing together innovative digital publishing with leading authors from the global scientific community.

Start exploring the collection-download the first chapter of every title for free.

IOP Publishing Nanotechnology

Nanotechnology 27 (2016) 254006 (7pp)

doi:10.1088/0957-4484/27/25/254006

# Hybrid silicon honeycomb/organic solar cells with enhanced efficiency using surface etching

#### Ruiyuan Liu, Teng Sun, Jiawei Liu, Shan Wu and Baoquan Sun

Jiangsu Key Laboratory for Carbon-Based Functional Materials and Devices, Institute of Functional Nano and Soft Materials (FUNSOM) and Collaborative Innovation Center of Suzhou Nano Science and Technology, Soochow University, Suzhou 215123, People's Republic of China

E-mail: bqsun@suda.edu.cn

Received 19 November 2015, revised 22 March 2016 Accepted for publication 13 April 2016 Published 16 May 2016



#### **Abstract**

Silicon (Si) nanostructure-based photovoltaic devices are attractive for their excellent optical and electrical performance, but show lower efficiency than their planar counterparts due to the increased surface recombination associated with the high surface area and roughness. Here, we demonstrate an efficiency enhancement for hybrid nanostructured Si/polymer solar cells based on a novel Si honeycomb (SiHC) structure using a simple etching method. SiHC structures are fabricated using a combination of nanosphere lithography and plasma treatment followed by a wet chemical post-etching. SiHC has shown superior light-trapping ability in comparison with the other Si nanostructures, along with a robust structure. Anisotropic tetramethylammonium hydroxide etching not only tunes the final surface morphologies of the nanostructures, but also reduces the surface roughness leading to a lower recombination rate in the hybrid solar cells. The suppressed recombination loss, benefiting from the reduced surface-to-volume ratio and roughness, has resulted in a high open-circuit voltage of 600 mV, a short-circuit current of 31.46 mA cm<sup>-2</sup> due to the light-trapping ability of the SiHCs, and yields a power conversion efficiency of 12.79% without any other device structure optimization.

Keywords: silicon nanostructures, hybrid solar cells, TMAH, surface etching, efficiency enhancement

(Some figures may appear in colour only in the online journal)

#### Introduction

Semiconductor nanostructures can reduce the volume of absorbers by providing excellent light absorption as well as light scattering and trapping. Solar cells with arrays of nanowires or nanoholes can also improve the carrier collection efficiency from a radial p—n junction geometry by decreasing the path length, which relaxes the quality demand of the materials. Silicon (Si) nanostructure-based photovoltaic devices have attracted wide interest due to their excellent optical and electrical performance [1–5]. There are various methods for fabricating Si nanostructures, including vapor-liquid-solid growth, supercritical-fluid-based growth, solution-based growth, reactive-ion etching,

electron beam lithography and metal-assisted chemical etching [6, 7].

Low-temperature-processed Si/polymer hybrid solar cells are intensively studied these days due to their unique advantages such as easy fabrication, potentially low cost and simple facility compared with the traditional Si solar cells. Si/poly (3, 4-ethylenedioxythiophene):polystyrenesulfonate (PEDOT:PSS) hybrid solar cells are specially favored due to the excellent properties of the polymer. Si nanowires [8–13], pyramids [14–16], nanocones [17] and hierarchical structures [18–20] are extensively adopted in the hybrid solar cell and considerable progress has been made with power conversion efficiencies (PCEs) of over 11%. However, nanostructure-based solar cells usually suffer from severe surface

recombination problems due to their high surface-to-volume (S/V) ratio property, which results in a relatively low opencircuit voltage  $(V_{oc})$  and a modest short-circuit current  $(J_{sc})$ . Most of the previously reported Si nanostructure-based hybrid solar cells exhibit  $V_{\rm oc}$  well below 600 mV, while their planar counterparts can show a  $V_{\rm oc}$  exceeding 640 mV [21, 22]. A hybrid Si nanocone/polymer solar cell with an efficiency of 11.10% shows a  $J_{\rm sc}$  of 29.60 mA cm<sup>-2</sup> due to the better antireflection and light-trapping properties, but only a  $V_{\rm oc}$  of 550 mV, even employing a highly doped n<sup>+</sup>-backside-field Si layer [17]. Si/PEDOT:PSS hybrid solar cells using hierarchical structures consisting of micropyramids and nanowires achieve an efficiency up to 11.48%, exhibiting a  $J_{\rm sc}$  of 34.46 mA cm<sup>-2</sup> and a  $V_{oc}$  of 520 mV [19]. A two-step surface treatment process is carried out to remove impurities and passivate the Si nanowires to reduce the recombination loss, and the Si nanowire/PEDOT:PSS hybrid device shows a higher  $V_{\rm oc}$  of 580 mV and a PCE of 12.4% [23]. For all these methods, either a complicated process or an unstable organic materials/SiO<sub>x</sub> layer is needed to address the recombination problem, which may hinder their future application.

In this study, we developed a Si honeycomb (SiHC) structure using nanosphere lithography and chemical surface etching, and this was demonstrated as a good nanostructure for hybrid Si/PEDOT:PSS solar cells. SiHC has shown enhanced light-trapping ability in comparison with the other Si nanostructures, and a much more robust structure compared with the relatively fragile nanowires or nanocones due to the conical-frustum geometry of each single unit. The anisotropic tetramethylammonium hydroxide (TMAH) etching not only tunes the surface morphologies of the nanostructures, but also smoothes the surface, thus resulting in a lower recombination rate in the hybrid solar cells. It has been reported that a nanostructure-based all-inorganic black-Si solar cell has achieved a confirmed 18.2% efficiency by suppressing Auger recombination in the heavy doping region and simultaneously controlling surface area by TMAH etching [2]. In our hybrid SiHC/PEDOT:PSS solar cells, the suppressed recombination loss benefiting from the reduced S/V ratio and roughness has resulted in a high  $V_{\rm oc}$  of 600 mV, a  $J_{\rm sc}$  of 31.46 mA cm<sup>-2</sup> due to the light-trapping ability of the SiHCs, and a PCE of 12.79% is yielded under air mass (AM) 1.5 G illumination without any other device structure optimization. A 59% enhancement in efficiency has been achieved compared with the hybrid solar cell without TMAH treatment, and the  $V_{\rm oc}$  is one of the record values for reported Si nanostructure/PEDOT:PSS solar cells.

#### **Experiments**

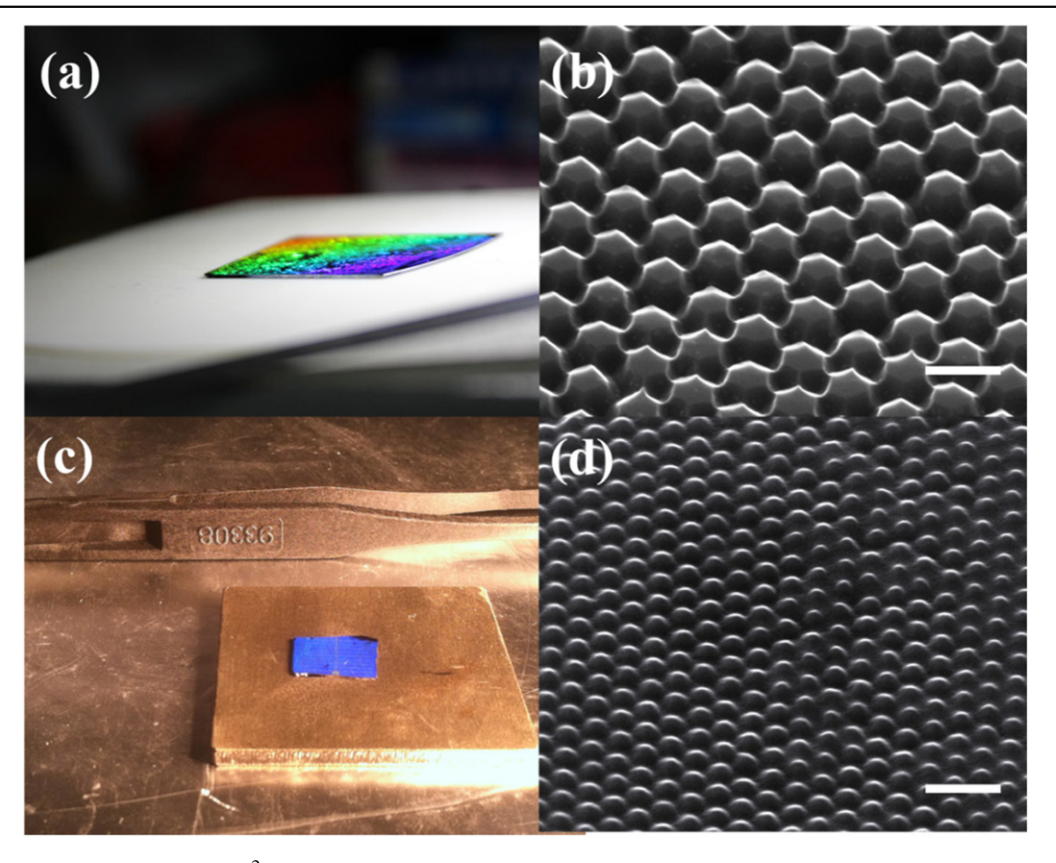
For SiHC nanostructure fabrication, hexagonal close-packed monolayer polystyrene (PS) nanospheres (360 nm in diameter, Nano-Micro Tech) were self-assembled on the surface of water and then loaded onto a 300  $\mu$ m n-type Si (100) substrate with a resistivity of 0.05  $\sim$  0.1  $\Omega$  cm. All the Si substrates were previously ultrasonically cleaned in acetone, ethanol and deionized (DI) water for 20 min, followed by

immersion into a piranha solution of H<sub>2</sub>SO<sub>4</sub>/H<sub>2</sub>O<sub>2</sub> at 115 °C for 1 h to ensure hydrophilic surfaces without any residual material. After the evaporation of water, the PS nanosphereloaded wafer was then transferred into the chamber of an inductively coupled plasma (ICP) etcher (Oxford Instrument, Plasmalab 80 plus). The SiHCs with PS tips were fabricated using a mixture of SF<sub>6</sub> (40 sccm), CF<sub>4</sub> (30 sccm) and O<sub>2</sub> (10 sccm) gases at a radio frequency power of 150 W and process pressure of 50 mTorr. The samples were subsequently ultrasonically treated in chloroform for 20 min to remove the PS residuals and cleaned in a piranha solution. The as-treated samples were then rinsed by deionized water and immersed into 5 vol% HF buffered solution for 5 min to remove the SiO<sub>x</sub> on the Si surface. Then, 1 vol% TMAH solution was used at room temperature to decrease the surface area and roughness of the Si nanostructures for different times. The asprepared SiHCs were spin-coated with highly conductive PEDOT:PSS (Clevios PH1000) mixed with 5 wt% dimethyl sulfoxide (DMSO) and 1 wt% Triton X-100 (surfactant) at 3000 rpm for 1 min, and then annealed at 125 °C for 20 min in glovebox. Finally, 200 nm-thick silver finger grids with a shading ratio of ~10% were thermally evaporated onto PEDOT:PSS as the front electrode and 200 nm-thick aluminum as the rear contact, with a total active area of 0.5 cm<sup>2</sup>.

The morphology of SiHCs on the planar Si substrate was characterized with a FEI Quanta 200 FEG high-resolution scanning electron microscope (SEM). Reflection spectra were measured using an integrating sphere (PerkinElmer Lambda 700). Solar cell characteristics were tested by a source meter (Keithley 2612) and a solar simulator (Newport 91160) under AM 1.5 G conditions at an illumination intensity of 100 mW cm<sup>-2</sup>, calibrated by a Newport standard Si solar cell (91150). A Newport monochromator 74125 and power meter 1918 with Si detector 918D were used to measure the external quantum efficiency (EQE). Minority carrier lifetime was based on a microwave detected photoconductance (MDP) technique with steady-state photogeneration (MDPmap, Freiberg Instruments GmbH).

#### **Results and discussion**

Figures 1(a) and (b) show a  $4 \times 4$  cm<sup>2</sup> Si substrate with SiHC and the corresponding SEM image of the SiHC structures. The color gradient is due to white light scattering in the periodic honeycomb arrays, demonstrating the excellent uniformity of the structures. The SEM image clearly shows not only the high order of the hexagonally distributed SiHC, but also the good surface morphology after TMAH treatment, which will be discussed later. The device with electrodes appears blue under 45-degree lamp illumination (figure 1(c), but changes color when the light incident angle is changed. Figure 1(d) shows the SEM image of SiHC coated with PEDOT:PSS in the hybrid device, which indicates a uniform film coverage of the honeycomb structures. This is attributed to the additional advantage which the flat-top surface of the structures has over the tapered nanocone or nanowire geometry.



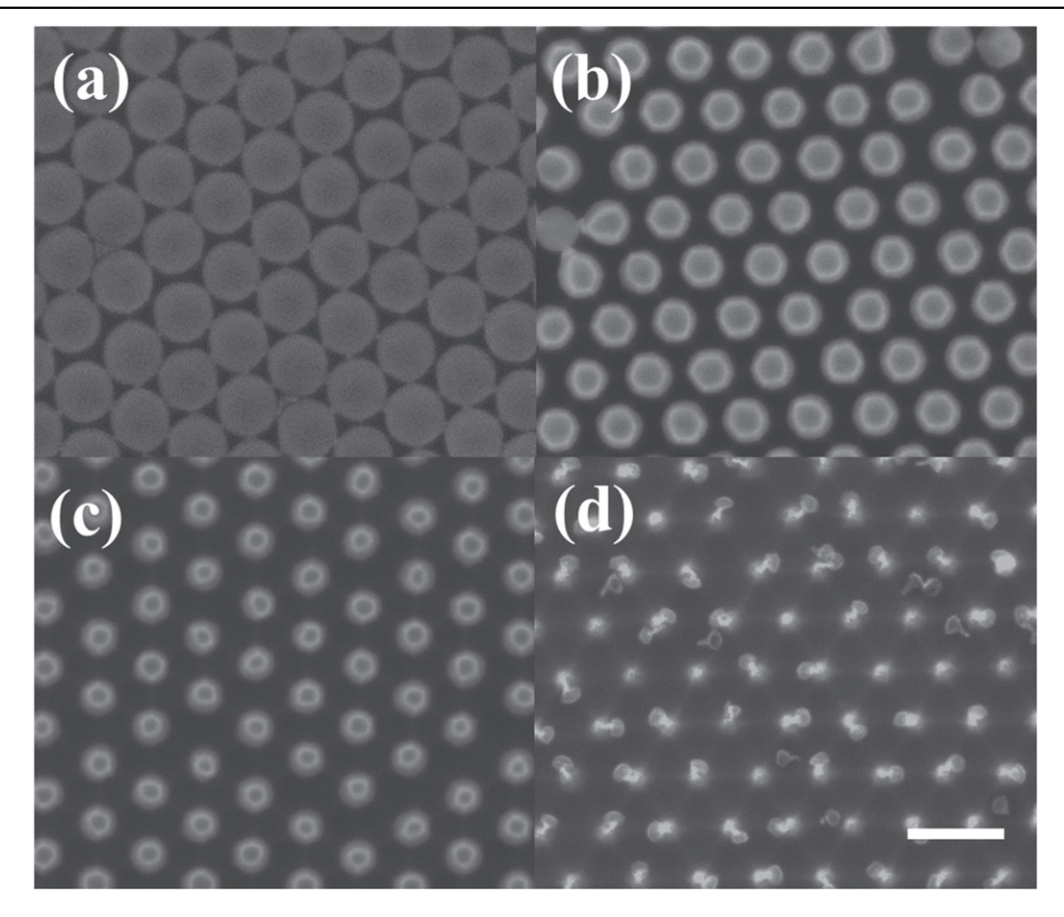
**Figure 1.** (a) Optical image of a  $4 \times 4$  cm<sup>2</sup> substrate with SiHC and (b) the corresponding SEM image after treatment in TMAH solution; (c) optical digital image of a hybrid solar cell under 45-degree lamp illumination and (d) the corresponding SEM image. The scale bars are 500 nm for (b) and 1  $\mu$ m for (d), respectively.

Figure 2 shows the top-view SEM images of the asfabricated SiHCs with PS on the top using different plasma treating times. The diameters of the PS nanospheres slightly decrease when the etching time is 30 s, but the close-packed morphology tends to become unclosed and the exposed Si is being etched, as shown in figure 2(a). When the etching time increases to 90 s, the diameters of the nanospheres as well as the top part of the SiHCs apparently decrease to ~160 nm (figure 2(b)). In this process, the increase of the plasmaetching time not only etches away the PS, but also the sidewalls of the SiHC. The diameters of the PS decrease to  $\sim$ 80 nm after 120 s etching, and when the time is 150 s, the PS along with the SiHCs are almost etched off with only tiny residuals left. The reflectance of the sample increases rapidly according to its visually shallow color (figures 2(c), (d)). This shows the good uniformity as well as the precise size control of the as-fabricated SiHCs.

Physical etching methods, such as the use of plasma, always result in a rough surface along the sidewalls of the nanostructures. The reactive-ion etching induced surface damage is also considered to deteriorate the short-wavelength photocurrent response and decrease the  $V_{\rm oc}$  of a solar cell [24]. Surface cleaning and TMAH wet etching are employed to remedy surface imperfections in order to improve the electrical properties. Figures 3(a) and (d) show a top view and 45-degree-tilted view of the SEM images of the SiHCs after plasma etching for 90 s. The diameters of the top part of the

SiHC are slightly smaller than the PS nanospheres due to the sidewall etching of the Si. Some pinholes are observed at the bottom part of the structures, as pointed out by the red circle in figure 3(b). The surface is relatively rough after plasma etching and surface cleaning (figure 3(e)). There are two main differences before and after 60 s TMAH wet etching for SiHC nanostructures. First, the edges of adjacent units increase and the top part becomes tapered; second, the sidewalls are smoother (figures 3(c), (f)). The morphology changes offer a few advantages: a wider spacing between adjacent units favors better infiltration of PEDOT:PSS since the polymer is macromolecular and can hardly penetrate into the narrow adjacent space of the nanostructures. Widening the adjacent nanostructure unit space improves the physical contact between Si and the organic layer. In addition, the smoother surface and lower surface-to-volume (S/V) ratio can dramatically reduce the recombination rate, which can eventually improve the device performance.

Figure 4 depicts the effects of different TMAH etching times on the electrical and optical properties of SiHC hybrid solar cells (0 s, 30 s, 60 s, 90 s). The electrical output characteristics of the cells are extracted by measuring the current density–voltage (J–V) characteristics, both under simulated AM 1.5 illumination at 100 mW cm<sup>-2</sup> and in the dark. Figure 4(a) shows the J–V characteristics of the SiHC hybrid solar cells with and without TMAH etching and the photovoltaic parameters are summarized in table 1. Without TMAH



**Figure 2.** Top-view SEM images of the as-fabricated SiHCs with PS under different plasma-etching times. (a) 30 s; (b) 90 s; (c) 120 s; (d) 150 s. The scale bars are 500 nm in all images.

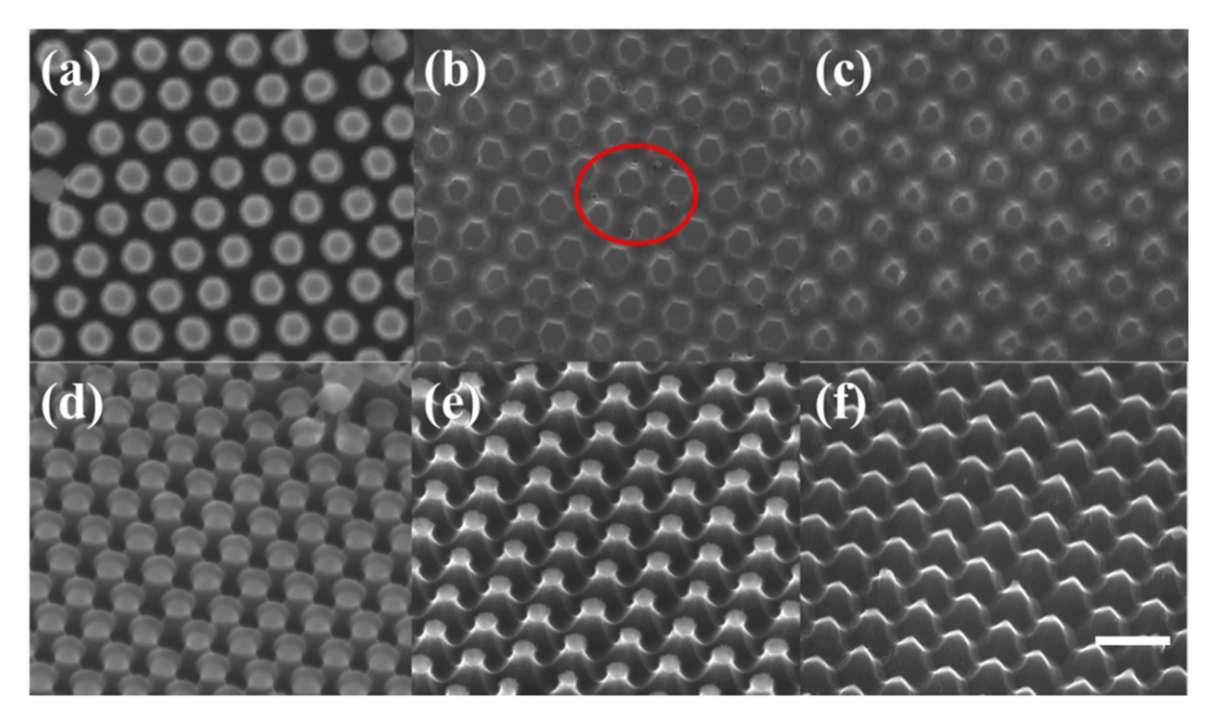


**Figure 3.** SEM images of the SiHC in different fabrication processes. (a) Top view and (d) 45-degree-tilted view of honeycomb arrays with PS after 90 s plasma etching; (b) top view and (e) 45-degree tilted view of honeycomb arrays without PS corresponding to (a) and (d); (c) top view and (f) 45-degree-tilted view of honeycomb arrays after 60 s TMAH etching corresponding to (b) and (e). The scale bars are 500 nm in all images. The red circle in (b) points out some pinholes left at the bottom part of the nanostructures after plasma etching.

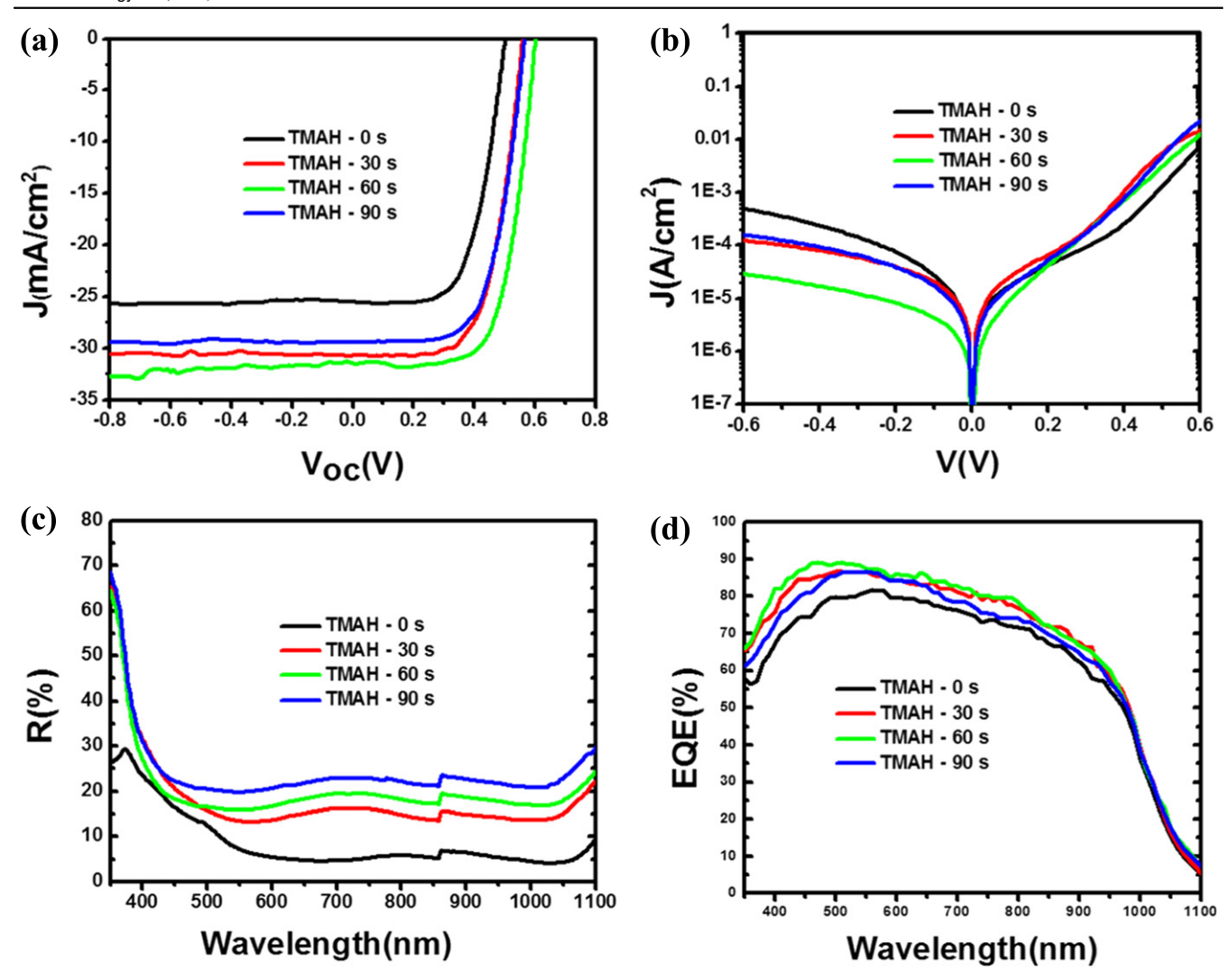


**Figure 4.** TMAH etching time versus electrical and optical properties of SiHC hybrid solar cells. TMAH etching times are 0 s, 30 s, 60 s and 90 s, respectively. (a) *J–V* characteristics under simulated AM 1.5 illumination of SiHC hybrid solar cells; (b) log *J-V* characteristics of the SiHC hybrid solar cells in the dark; (c) reflectance spectra of SiHCs; (d) EQE spectra of the SiHC hybrid solar cells.

**Table 1.** Electrical output characteristics of the hybrid cells<sup>a</sup>, the corresponding minority carrier lifetime and the surface-to-volume (S/V) ratio of the Si samples based on different TMAH etching times.

Etching Time (s)	V <sub>oc</sub> (mV)	$J_{\rm sc}~({\rm mA~cm}^{-2})$	Fill Factor	PCE (%)	$T_{\rm eff}~(\mu {\rm s})$	S/V Ratio
0	500	25.52	0.63	8.02	7.6	1.70
	$493 \pm 5.19$	$25.31 \pm 0.16$	$0.61 \pm 0.010$	$7.61 \pm 0.50$		
30	559	30.73	0.64	11.01	9.0	1.65
	$552\pm6.33$	$30.31 \pm 0.31$	$0.63 \pm 0.006$	$10.56 \pm 0.41$		
60	600	31.46	0.67	12.79	10.4	1.42
	$594\pm5.52$	$30.99 \pm 0.17$	$0.66 \pm 0.009$	$12.11 \pm 0.56$		
90	559	29.43	0.66	10.89	9.5	1.52
	$555\pm3.89$	$28.68 \pm 0.25$	$0.64 \pm 0.013$	$10.22\pm0.34$		

<sup>&</sup>lt;sup>a</sup> Data and statistics are based on five devices for each condition. Numbers in bold are the maximum values.

etching, the hybrid solar cell exhibits a  $V_{\rm oc}$  of 500 mV, a  $J_{\rm sc}$  of 25.52 mA cm<sup>-2</sup>, and a fill factor (FF) of 0.63, resulting in an overall PCE of 8.02%. Even the reflectance of the untreated SiHC structures is as low as 10% from a 500 nm to 1100 nm wavelength (figure 4(c)); the  $J_{\rm sc}$  is still low due to the recombination-induced current loss as well as poor contact

between Si and PEDOT:PSS. The  $V_{\rm oc}$  increases to 559 mV after a 30 s etching time and saturates at 600 mV for an etching time of 60 s. The  $J_{\rm sc}$  also increases by 20% after 30 s of TMAH etching, growing to 31.46 mA cm<sup>-2</sup> after 60 s of etching, which is a 23% increase. With improvements in the  $V_{\rm oc}$ ,  $J_{\rm sc}$  and FF, the SiHC hybrid solar cell etched for 60 s

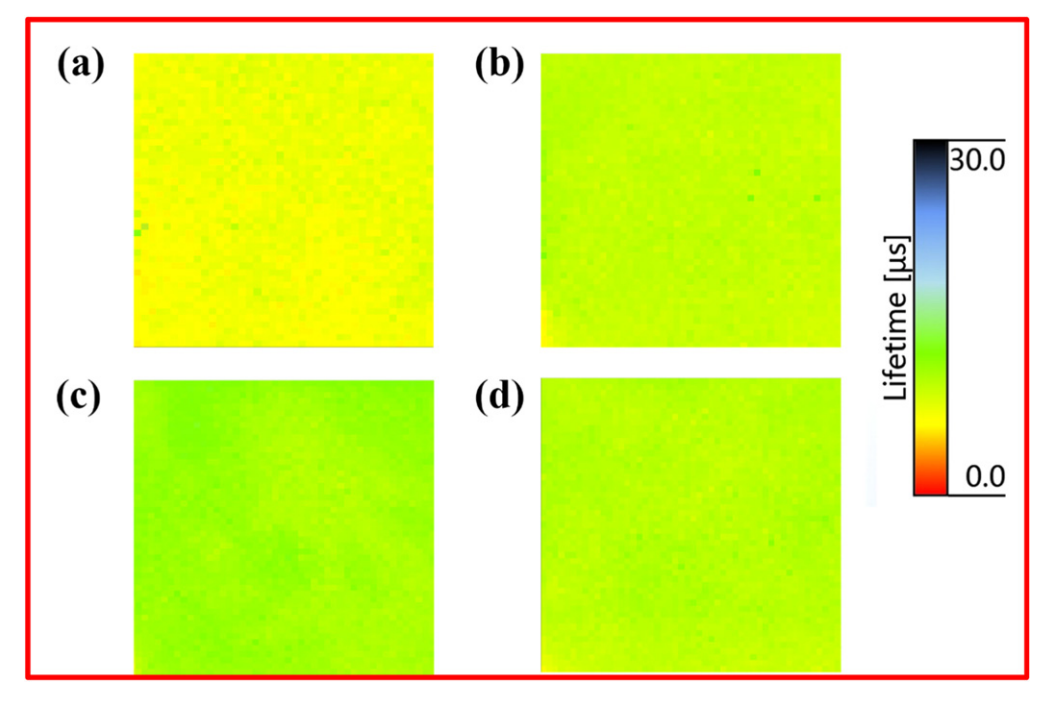


**Figure 5.** Minority carrier lifetime mapping of four samples with different TMAH etching times of (a) 0 s; (b) 30 s; (c) 60 s; (d) 90 s. All sample sizes are 1 cm × 1 cm.

yields a PCE of 12.79%, exhibits a 59% efficiency enhancement. However, a longer etching time of 90 s results in a decline of the performance, partially due to the increasing reflectance (figure 4(c)). The corresponding J-V characteristics measured in the dark are shown in figure 4(b). The current densities in forward and reverse bias of the device with TMAH etching are lower for devices without etching, which result from the lower carrier recombination rate at the organic-Si interface with reduced roughness, and the lower saturation current density eventually leads to a larger  $V_{\rm oc}$ . The improvement in the  $J_{\rm sc}$  could also be attributed to the following reasons in our case: light-trapping ability combined with reduced surface recombination rate. Figure 4(c) shows the reflectance spectra of the SiHC with and without TMAH etching. The reflectance of the nanostructures increases rapidly at around 350 nm wavelength after TMAH etching, and becomes stable at ~17% and ~20% in a wavelength range from 450 nm to 1100 nm for 30 s and 60 s etching, respectively. The variation in reflectance probably arises from the reduced diameter and tapered top of the SiHC nanostructures. This demonstrates that the light-trapping ability of the nanostructures is weakening instead of becoming stronger after the etching, which excludes the light-enhanced element in the current. Inspection of the external quantum efficiency (EQE) shown in figure 4(d) confirms the  $J_{sc}$  enhancement after TMAH etching, even with a higher reflectance. We hence attribute the increased  $J_{\mathrm{sc}}$  to the reduced surface recombination rate of the device, which results both from the reduced surface recombination of the nanostructures and the better physical contact with PEDOT:PSS.

To analyze the effects of TMAH etching on the electrical properties of a nanostructured surface, spatial mapping of the minority carrier lifetime ( $\tau_{\rm eff}$ ) measurements were carried out. The measured  $\tau_{\rm eff}$  in Si are lifetimes consisting of bulk and surface components, expressed as  $1/\tau_{\rm eff} = 1/\tau_{\rm bulk}$  +  $(S_{\rm eff}^{\rm F} + S_{\rm eff}^{\rm B})/d$ , where  $au_{
m bulk}$  is the Shockley-Read-Hall bulk recombination lifetime,  $S_{eff}^{F}$  and  $S_{eff}^{B}$  are the effective surface recombination velocities at the front and back surfaces, respectively, and d is wafer thickness. Since all samples use the same wafer and are treated in the identical plasma conditions, the variations of measured lifetime should reveal the front-surface recombination properties which are determined by the TMAH etching time. As shown in figure 5 and table 1, the minority carrier lifetime of the sample without TMAH etching is 7.6  $\mu$ s, corresponding to an S/V ratio of 1.70. Once etched in TMAH for 30 s, most of the plasma-induced roughness and flaws are trimmed off by the gentle chemical wet etching, and the S/V ratio decreases to 1.65, accompanied by an improved carrier lifetime of 9.0  $\mu$ s. The carrier lifetime of the sample etched for 60 s increases to 10.4  $\mu$ s due to the reduced surface defects, which results from both the reduced S/V ratio (1.42) and the smoothed nanostructure surface. But longer time treatment will subsequently lower the lifetime due to the further etching of the bottom gaps of the nanostructures, which could offset the benefits from the nanostructure itself. The carrier lifetime of the sample falls slightly to 9.5  $\mu$ s after etching for 90 s, along with an S/V ratio of 1.52. This may well explain the  $V_{\rm oc}$  dependence of the hybrid solar cell on etching time. Up to a certain level, the output property of a solar cell depends on many complicated elements. In our case, the final performance of the hybrid solar cell is mainly determined by the trade-off between surface recombination and light reflection.

#### Conclusion

In conclusion, we have demonstrated a novel SiHC nanostructure and shown its application in a SiHC/PEDOT:PSS hybrid solar cell. The highly periodic nanostructure array is fabricated by a combination of a facile nanosphere lithography process and TMAH post-wet etching. The surface roughness of the nanostructures is greatly reduced and a low S/V ratio is achieved after a 60 s wet etching. All of the parameters of the disposed hybrid devices are improved due to better physical contact and a lower surface recombination rate. An enhanced efficiency of 12.79% was achieved with a high  $V_{\rm oc}$  of 600 mV due to the improved junction quality, a  $J_{\rm sc}$  of 31.46 mA cm<sup>-2</sup> from the good light-trapping ability of the SiHCs, and a modest FF of 0.67. An improvement of 59% has been achieved compared to devices without wet etching, which demonstrates the benefits of the facile post-treating process. We believe that the hybrid solar cells would be further improved by optimizing the geometries of the honeycomb arrays, the contact with electrodes and the properties of the polymer.

#### **Acknowledgments**

This work was supported by the National Basic Research Program of China (973 Program) (No. 2012CB932402), the National Natural Science Foundation of China (Nos. 91333208, 61176057), the Priority Academic Program Development of Jiangsu Higher Education Institutions (PAPD) and the Collaborative Innovation Center of Suzhou Nano Science and Technology.

#### References

- Garnett E and Yang P 2010 Light trapping in silicon nanowire solar cells *Nano Lett.* 10 1082
- [2] Oh J, Yuan H-C and Branz H M 2012 An 18.2%-efficient black-silicon solar cell achieved through control of carrier recombination in nanostructures Nat. Nanotechnol. 7 743
- [3] Peng K-Q, Wang X, Li L, Wu X-L and Lee S-T 2010 Highperformance silicon nanohole solar cells J. Am. Chem. Soc. 132 6872
- [4] Kelzenberg M D, Turner-Evans D B, Kayes B M, Filler M A, Putnam M C, Lewis N S and Atwater H A 2008 Photovoltaic measurements in single-nanowire silicon solar cells *Nano Lett.* 8 710
- [5] Tsakalakos L, Balch J, Fronheiser J, Korevaar B, Sulima O and Rand J 2007 Silicon nanowire solar cells *Appl. Phys. Lett.* 91 233117
- [6] Peng K-Q and Lee S-T 2011 Silicon nanowires for photovoltaic solar energy conversion Adv. Mater. 23 198
- [7] Huang Z, Geyer N, Werner P, de Boor J and Gösele U 2011 Metal-assisted chemical etching of silicon: a review Adv. Mater. 23 285

- [8] Shen X, Sun B, Liu D and Lee S-T 2011 Hybrid heterojunction solar cell based on organic–inorganic silicon nanowire array architecture J. Am. Chem. Soc. 133 19408
- [9] He L, Rusli, Jiang C, Wang H and Lai D 2011 Simple approach of fabricating high efficiency Si nanowire/ conductive polymer hybrid solar cells *IEEE Electron Device Lett.* 32 1406
- [10] Zhang F, Song T and Sun B 2012 Conjugated polymer-silicon nanowire array hybrid Schottky diode for solar cell application *Nanotechnology* 23 194006
- [11] Yu P et al 2013 13% Efficiency hybrid organic/siliconnanowire heterojunction solar cell via interface engineering ACS Nano 7 10780
- [12] Moiz S A, Nahhas A M, Um H-D, Jee S-W, Cho H K, Kim S-W and Lee J-H 2012 A stamped PEDOT: PSS– silicon nanowire hybrid solar cell *Nanotechnology* 23 145401
- [13] Sharma M, Pudasaini P R, Ruiz-Zepeda F, Elam D and Ayon A A 2014 Ultrathin, flexible organic-inorganic hybrid solar cells based on silicon nanowires and PEDOT: PSS ACS Appl. Mater. Interfaces 6 4356
- [14] Chen T-G, Huang B-Y, Chen E-C, Yu P and Meng H-F 2012 Micro-textured conductive polymer/silicon heterojunction photovoltaic devices with high efficiency *Appl. Phys. Lett.* 101 033301
- [15] Schmidt J, Titova V and Zielke D 2013 Organic-silicon heterojunction solar cells: Open-circuit voltage potential and stability Appl. Phys. Lett. 103 183901
- [16] Chen T-G, Huang B-Y, Liu H-W, Huang Y-Y, Pan H-T, Meng H-F and Yu P 2012 Flexible silver nanowire meshes for high-efficiency microtextured organic-silicon hybrid photovoltaics ACS Appl. Mater. Interfaces 4 6857
- [17] Jeong S, Garnett E, Wang S, Yu Z, Fan S, Brongersma M L, McGehee M D and Cui Y 2012 Hybrid silicon nanoconepolymer solar cells *Nano Lett.* 12 2971
- [18] He L, Lai D, Wang H, Jiang C and Rusli 2012 High-efficiency Si/polymer hybrid solar cells based on synergistic surface texturing of Si nanowires on pyramids Small 8 1664
- [19] Wei W-R, Tsai M-L, Ho S-T, Tai S-H, Ho C-R, Tsai S-H, Liu C-W, Chung R-J and He J-H 2013 Above-11%efficiency organic—inorganic hybrid solar cells with omnidirectional harvesting characteristics by employing hierarchical photon-trapping structures *Nano Lett.* 13 3658
- [20] Thiyagu S, Hsueh C-C, Liu C-T, Syu H-J, Lin T-C and Lin C-F 2014 Hybrid organic–inorganic heterojunction solar cells with 12% efficiency by utilizing flexible film-silicon with a hierarchical surface *Nanoscale* 6 3361
- [21] Pietsch M, Jäckle S and Christiansen S 2014 Interface investigation of planar hybrid n-Si/PEDOT: PSS solar cells with open circuit voltages up to 645 mV and efficiencies of 12.6% Appl. Phys. A 115 1109
- [22] Liu R, Lee S-T and Sun B 2014 13.8% Efficiency hybrid Si/ organic heterojunction solar cells with MoO3 film as antireflection and inversion induced layer Adv. Mater. 26 6007
- [23] Wang J, Wang H, Prakoso A B, Togonal A S, Hong L and Jiang C 2015 High efficiency silicon nanowire/organic hybrid solar cells with two-step surface treatment *Nanoscale* 7 4559
- [24] Schaefer S and Lüdemann R 1999 Low damage reactive ion etching for photovoltaic applications J. Vac. Sci. Technol. A 17 749